Electronic Supporting Information

Polyoxometalate-based supramolecular porous frameworks with dual-active centers toward highly-efficient synthesis of functionalized *p*-benzoquinones

Shenzhen Chang, Yanhong Chen, Haiyan An,* Qingshan Zhu, Huiyun Luo, Yaohui Huang

State Key Laboratory of Fine Chemicals, School of Chemical Engineering, Dalian University of Technology, Dalian 116023, People's Republic of China.

CONTENTS

Section I. Supplementary Experimental Section

1.1 Materials and instrumentation.

$K_5[BW_{12}O_{40}]\cdot xH_2O$ and $K_5[SiW_{12}O_{40}]\cdot xH_2O$ were synthesized based on the literature method with slight modifications, which can also be proved by IR spectra.[S1] Other chemicals were used as purchased without purification. Elemental analyses (H, C and N) were performed on a Perkin-Elmer 2400 CHN elemental analyzer. IR spectra were recorded in the range 4000-400 cm^{-1} on a Nexus Euro FT/IR Spectrophotometer using KBr pellets. The powder X-ray diffraction (PXRD) patterns of the as-prepared products were carried out by using Rigaku SmartLab X-ray diffractometer with Cu-Kα radiation (λ = 0.154 nm) and 2θ transforming from 5 to 50°. The X-ray single crystal diffraction were collected by Bruker D8 Venture single crystal diffractometer with MoKα radiation. Diffuse reflectivity spectra were collected on a finely ground sample with a Cary 500 spectrophotometer equipped with a 110 mm diameter integrating sphere, which were measured from 200 to 800 nm. Liquid UV-vis spectrum was measured from 250 to 450 nm on Techcomp UV1000 spectrophotometer. ICP-AES was performed on Optima 7000 DV of Perkinelmer. Thermogravimetric (TG) analysis is performed on a TGA/DSC 3+ (Mettler Toledo) equipped with a DTA sensor in a nitrogen atmosphere at a rate of 10°C min^{-1}. The products in catalytic experiments were determined by gas chromatography with SE-54 capillary column (Techcomp GC 7900II) and gas chromatography-mass spectroscopy (Trace ISQ). The EDS were determined using a JSM-7610F Plus scanning electron microscope at an accelerating voltage of 10 kV. The fluorescence spectra were recorded on Hitachi F7000 spectrophotometer at 380 nm excitation wavelength.

1.2 Synthesis of $K_5[BW_{12}O_{40}]\cdot xH_2O$.

$Na_2WO_4\cdot 2H_2O$ (50 g, 0.15 mol) and H_3BO_3 (2.5 g, 0.04 mol) were dissolved in 50 mL of distilled water. Then 16 mL of concentrated hydrochloric acid was slowly added. The solution was allowed to boil for 3 h and removed the colorless solid from the bottom by suction filtration. The filtrate was heated and boiled for 0.5 h after adjusting the pH~2 with 6M HCl. Finally, 12 g of potassium chloride was added to obtain white precipitates, which were suction filtered and dried at room temperature. Yield: 65% (based on $Na_2WO_4\cdot 2H_2O$). IR (Fig. S12, KBr pellet, cm^{-1}): 1002 (w), 958 (s), 910 (s), 803 (s), 506 (m).

1.3 Synthesis of $K_4[SiW_{12}O_{40}]\cdot xH_2O$.

The synthesis of $K_4[SiW_{12}O_{40}]\cdot xH_2O$ is a two-step process. The first part is to synthesize $H_4SiW_{12}O_{40}\cdot xH_2O$ as follows: $Na_2WO_4\cdot 2H_2O$ (100 g, 0.30 mol) was dissolved in 200 mL of distilled water, and 20 mL of concentrated hydrochloric acid was slowly added dropwise. The solution was heated to boiling, and added 20 mL of concentrated hydrochloric acid again. Then 50 mL of sodium silicate hot solution ($Na_2SiO_3\cdot 9H_2O$, 7.5g, 0.026 mol) and 60 mL of concentrated hydrochloric acid were added. The solution was kept boiling for 0.5 h and then cooled to room temperature. The precipitate produced could be filtered out. The filtrate was transferred to a separatory funnel, and 40 mL of concentrated hydrochloric acid and 50 mL of ether were added. The solution was shaken evenly, and the bottom oily layer was drawn off. This complex was added a few drops of distilled water and dried in vacuum overnight to obtain a white solid ($H_4SiW_{12}O_{40}\cdot xH_2O$).

In the second stage, 25 g of $H_4SiW_{12}O_{40}\cdot xH_2O$ was added to 30 mL of distilled water, and heated to dissolve completely. Then 20 mL of 2 M KOH solution was added, heated to evaporate and crystallized, and finally a white solid was collected. Yield: 59% (based on $Na_2WO_4\cdot 2H_2O$). IR (Fig. S12, KBr pellet, cm^{-1}): 1019 (w), 980 (s), 920 (s), 882 (w), 789 (s), 536 (m).

1.4 Synthesis of $K_3(H_2O)_4[Cu(tza)_2(H_2O)]_2[Cu(Htza)_2(H_2O)_2][BW_{12}O_{40}]\cdot 6H_2O$ (1).

$K_5[BW_{12}O_{40}]\cdot xH_2O$ (0.25 g, ~0.080 mmol), Htza (0.07 g, 0.547 mmol) and $CuCl_2\cdot 2H_2O$ (0.090 g, 0.528 mmol) were dissolved in 25 mL of distilled water and stirred for 30 min. The pH of the resulting mixture was adjusted to 4.7 with 4 M KOH solution. After stirring for another 30 min, the mixture was heated and stirred for 3.5 h at 80 °C. Cooled to room temperature and filter, the filtrate was kept undisturbed for two weeks under ambient conditions. Blue striped crystals were obtained in about 32% yield (based on $K_5[BW_{12}O_{40}]\cdot xH_2O$). $C_{18}H_{48}N_{24}K_3Cu_3BW_{12}O_{66}$ (4181.52), found (calcd)%: C, 5.43 (5.17); H, 1.52 (1.16); N, 8.00 (8.04). IR (Fig. S12, KBr pellet, cm^{-1}): 3452 (s), 3134 (s), 3002 (s), 1621 (s), 1504 (m), 1453 (w), 1388 (s), 1298 (s), 1189 (m), 1103 (s), 999 (w), 955 (s), 905 (s), 826 (s).

1.5 Synthesis of $H_3K_3(H_2O)_3[Cu(Htza)_2(H_2O)]_3[SiW_{12}O_{44}]\cdot 14H_2O$ (2).

The synthesis process of **2** was similar to that of **1**, except that $K_5[SiW_{12}O_{40}]\cdot xH_2O$ (0.25 g, ~0.075 mmol) instead of $K_5[BW_{12}O_{40}]\cdot xH_2O$, and increase the mole ratio of copper salt in the system ($CuCl_2\cdot 2H_2O$, 0.180 g, 1.056 mmol). The pH value was

adjusted to 3.07 by adding 4 M KOH dropwise and the mixture was heated for 3.0 h at 80 °C. The resulting solution was cooled to room temperature and filtered, and left to evaporate at room temperature. Gem blue hexagonal crystals of **2** were obtained after several days. Yield: 36% (based on $K_5[SiW_{12}O_{40}]\cdot xH_2O$). $C_{18}H_{67}N_{24}K_3Cu_3SiW_{12}O_{76}$ (4377.94), found (calcd)%: C, 5.24 (4.94); H, 1.62 (1.54); N, 7.66 (7.68). IR (Fig. S12, KBr pellet, cm^{-1}): 3484 (s), 3141 (s), 2962 (s), 1641 (s), 1508 (m), 1429 (w), 1388 (s), 1305 (m), 1182 (m), 1148 (w), 1099 (s), 1015 (w), 973 (m), 924 (s), 884 (w), 800 (s), 699 (w).

1.6 X-Ray crystallography.

The crystal data of **1** and **2** were collected at 190(2) K with graphite monochromatic Mo Kα radiation (λ = 0.71073 Å). The crystal structures were solved and refined by full matrix least-squares methods against F^2 by using SHELXTL-2018 programs.[S ( )] All non-hydrogen atoms were refined with anisotropic temperature parameters. All hydrogen atoms associated with C and N atoms were placed in geometrically idealized positions using a riding model. Crystallographic data, structure refinements and CCDC reference numbers for **1** and **2** are listed in Table S6.

1.7 General methods for catalyzing oxidation.

The oxidation experiments were carried out in a glass reactor (1.5 mL), equipped with magnetic stirrer (600 rpm) and temperature control. The catalytic activities of **1** and **2** were first evaluated in the oxidations of 2,3,6-TMP (0.1 or 0.25 mmol). The effect of catalyst (0.25−0.625 μmol), oxidants (≥65 % tert-butyl hydroperoxide: 0.50−0.70 mmol), temperature (r.t.–80 °C) as well as solvents (0.5 mL) were analyzed. The reactions were started with the addition of TBHP to a mixture of 0.5 mL solvent containing substrates and catalysts **1** and **2**. The reaction products were identified by GC/MS and ^{1}H NMR and quantified by GC using naphthalene as internal standard. Before recycle, the catalyst was separated by filtration, washed with MeCN, and dried in vacuum at 60 °C. In multi-cycle continuous experiment, the initial mol of phenol and TBHP were maintained at 0.25 mmol and 0.55 mmol by continuous addition after the reaction in the previous cycle. Blank experiments in the absence of catalyst, TBHP or both were also carried out at similar conditions.

1.8 General methods for detecting TBHP.

The standard curve of TBHP was established at 40 °C for 5 min. Typically, 3,3′,5,5′-tetramethylbenzidine (TMB, 3.12 μmol) and TBHP (0.25-2.03 μmol) were added into

3 mL of acetate buffer solution (pH~3.95) in turn, and the resulting mixture was stirred at 40 °C for 5 min, and then filtered using a syringe filter immediately. The absorbance of the filtrates at 661 nm was measured on UV-vis spectrophotometer to evaluate the 3,3',5,5'-tetramethyl-[1,1'-bi(cyclohexylidene)]-2,2',5,5'-tetraene-4,4'-diiminium (oxTMB) content.

For TBHP detection after catalytic reaction. The reaction system was quickly filtered with a syringe filter to remove the catalysts, and 30 μL of the filtrate was added to 3mL of acetic acid buffer (pH~3.95) containing 3.12 μmol of TMB. The resulting mixture was stirred at 40 °C for 5 min, and then filtered again using a syringe filter immediately. The absorbance of the filtrates at 661 nm was measured on UV-vis spectrophotometer to evaluate the oxTMB content.

1.9 Calculations of oxidant utilization efficiency

TBHP efficiency (%) = 100 × [mol of TBHP consumed in the formation of TMBQ/mol of TBHP converted]

(i) Mol of TBHP consumed in the formation of TMBQ = 2 × mol of TMBQ[a].

(ii) Mol of TBHP converted = total mol of TBHP has been originally used – the remaining mol of TBHP in the system after the reaction[b].

[a]According to the reaction stoichiometry, TMP oxidation to TMBQ requires 2 equivalents of TBHP.

[b]The remaining mol of TBHP in the system after the reaction was estimated by the UV-Vis spectrophotometry and detailed experimental operations see "*1.8 General methods for detecting TBHP*".

Section II. Supplementary Structure Figures

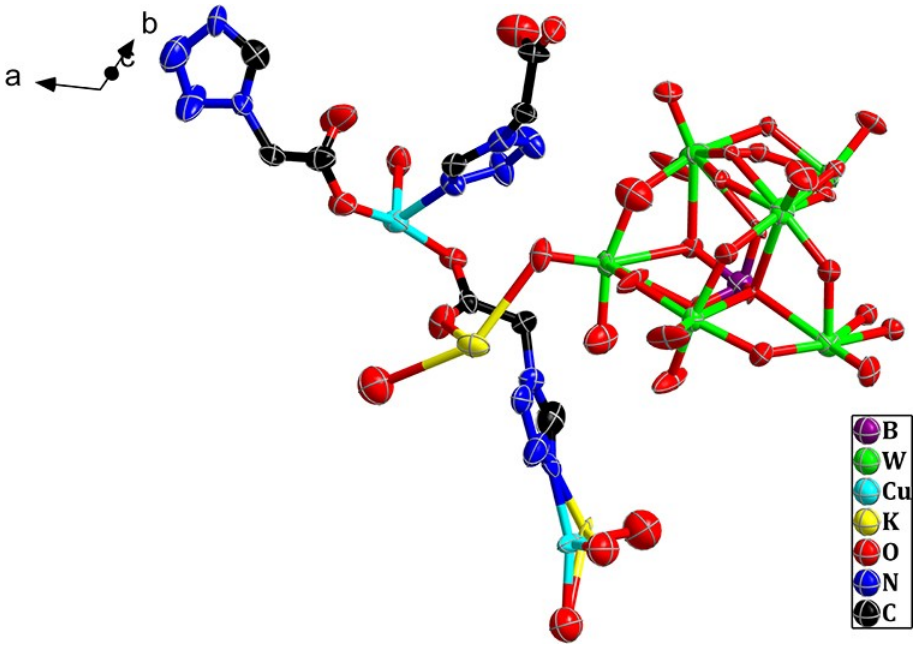

Fig. S1. ORTEP drawing of **1** with thermal ellipsoids at 50% probability.

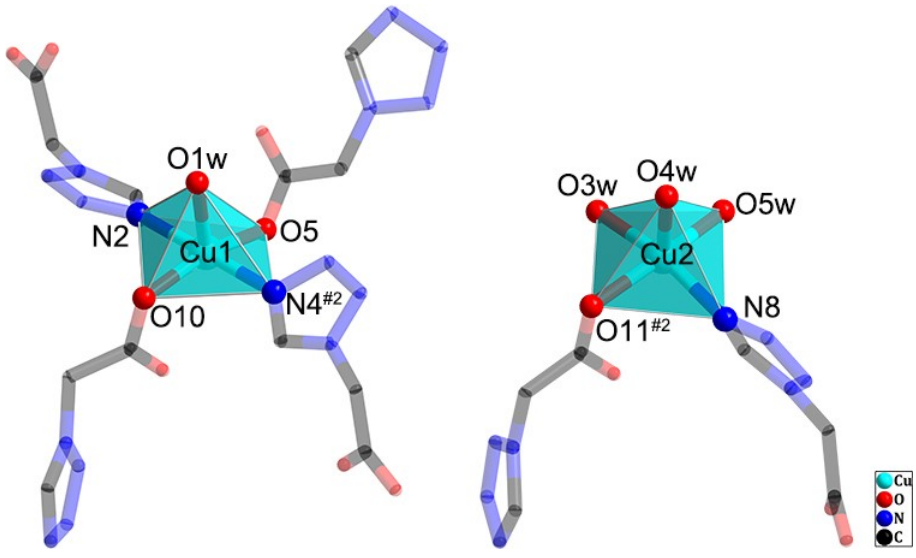

Fig. S2. The coordination modes of Cu1 (left), and Cu2 (right) in **1**. The "w" refers to coordination water molecules and the symmetry transformations used to generate equivalent atoms: #2: x-y, x-1, -z+2.

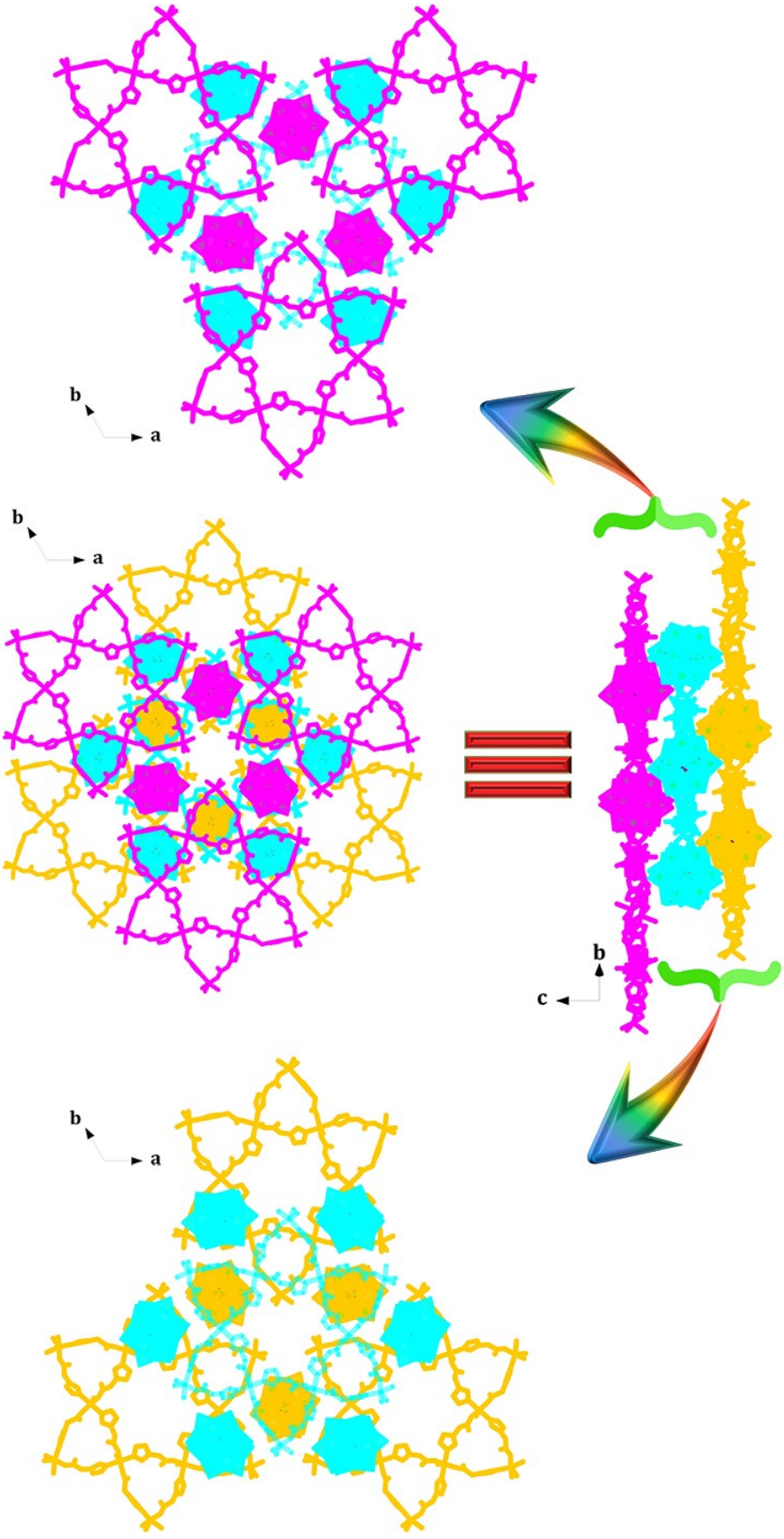

Fig. S3. The interaction mode between BW_{12} anion and metal-organic units in **1**.

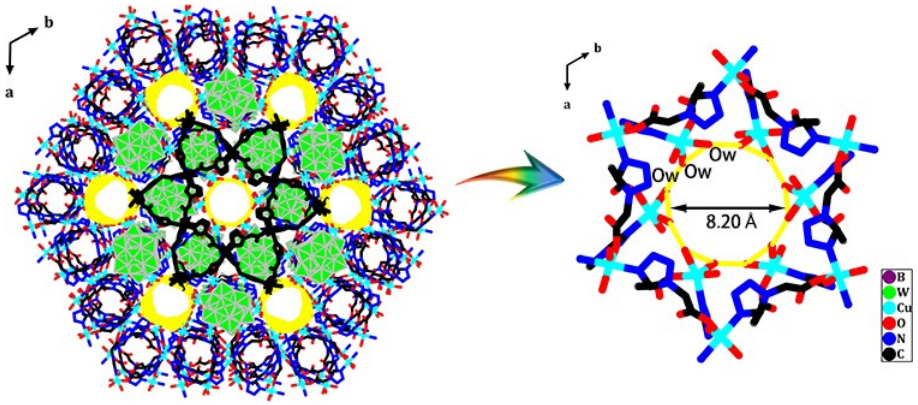

Fig. S4. The available channels in **1**. The "Ow" refers to coordination water molecules.

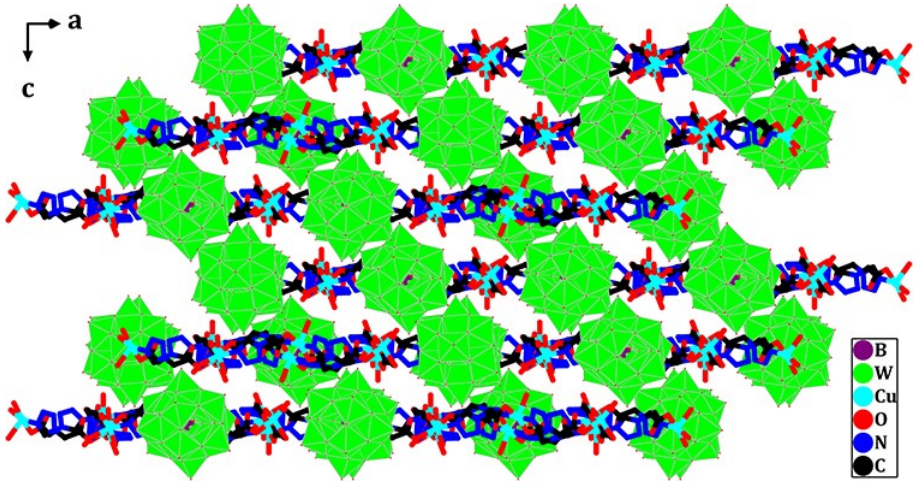

Fig. S5. The POM-based 3D supramolecular structure of **1** viewed from the *b* axis.

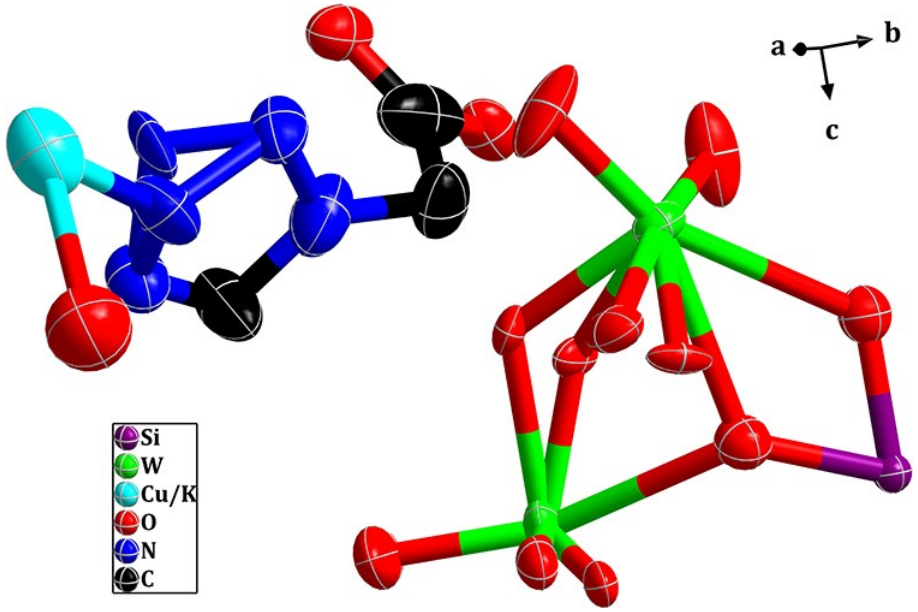

Fig. S6. ORTEP drawing of **2** with thermal ellipsoids at 50% probability**.**

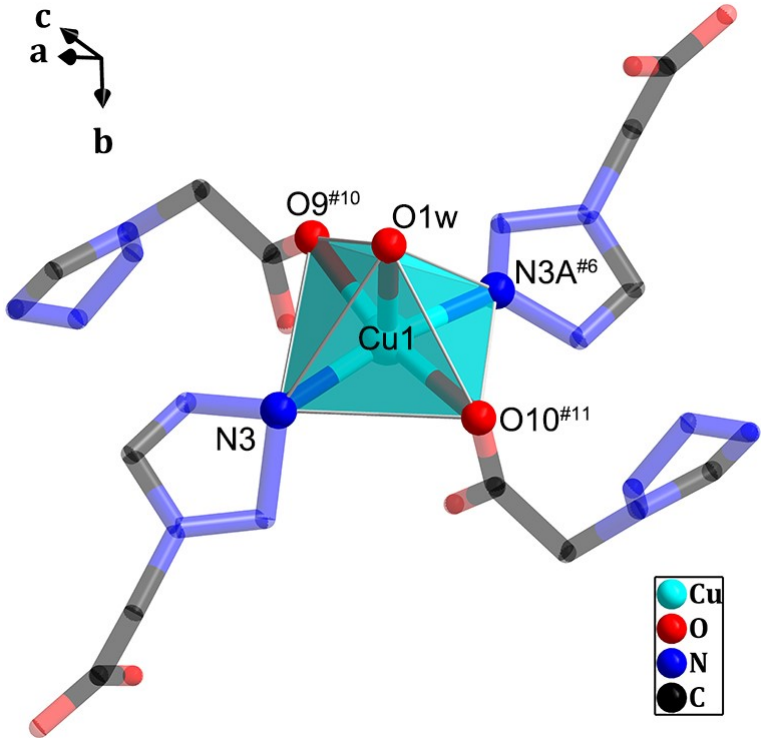

Fig. S7. The coordination modes of Cu1 in **2**. The "w" refers to coordination water molecules and the symmetry transformations used to generate equivalent atoms: #6 -x+1, -y+1, -z+2; #10 -y+1, x-y+1, z; #11 y, -x+y, -z+2.

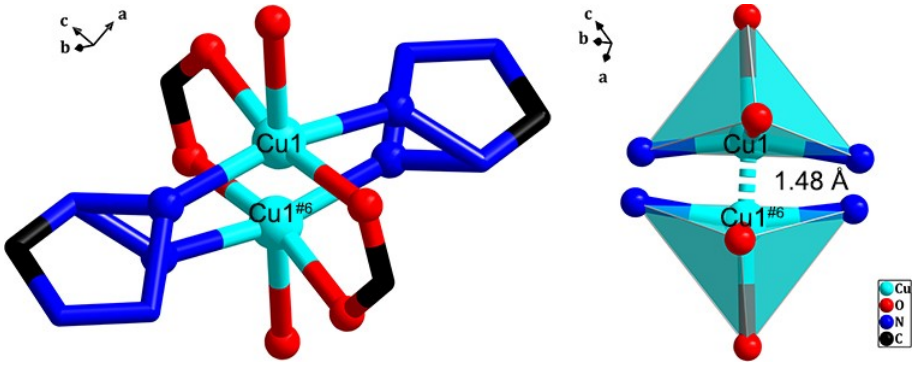

Fig. S8. Pseudo-dimeric cupric dicarboxylate units based on disorder Cu1 in **2**. The symmetry transformations used to generate equivalent atoms: #6 -x+1, -y+1, -z+2.

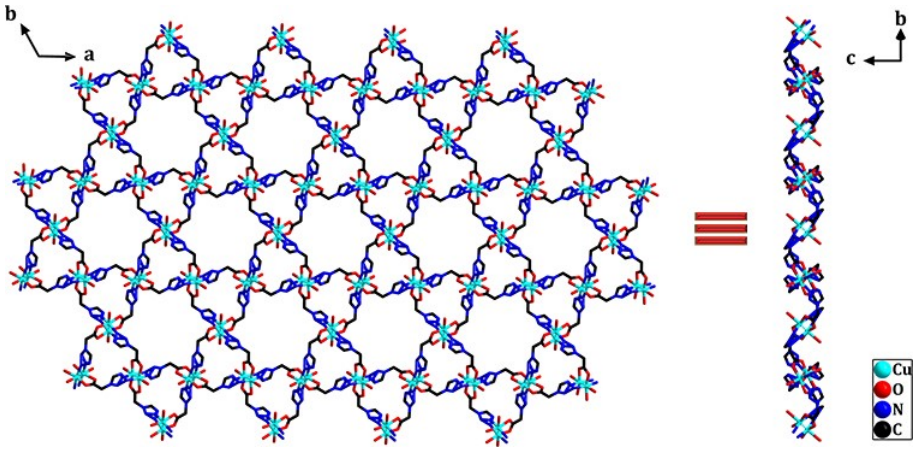

Fig. S9. The 2D metal organic layer in **2**.

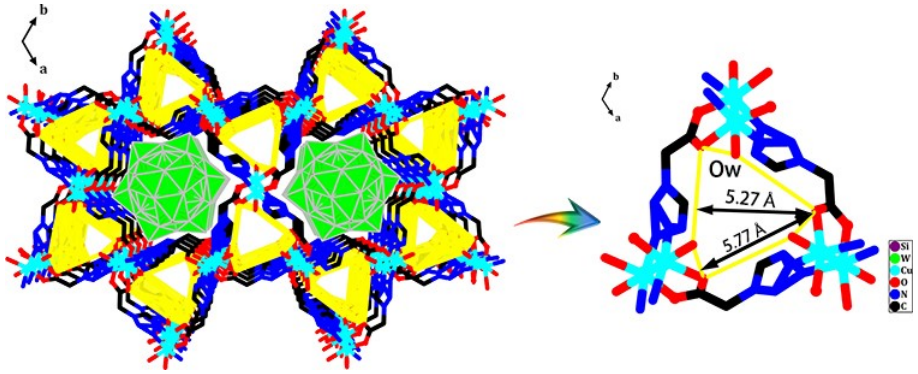

Fig. S10. The available channels in **2**. The "Ow" refers to coordination water molecules.

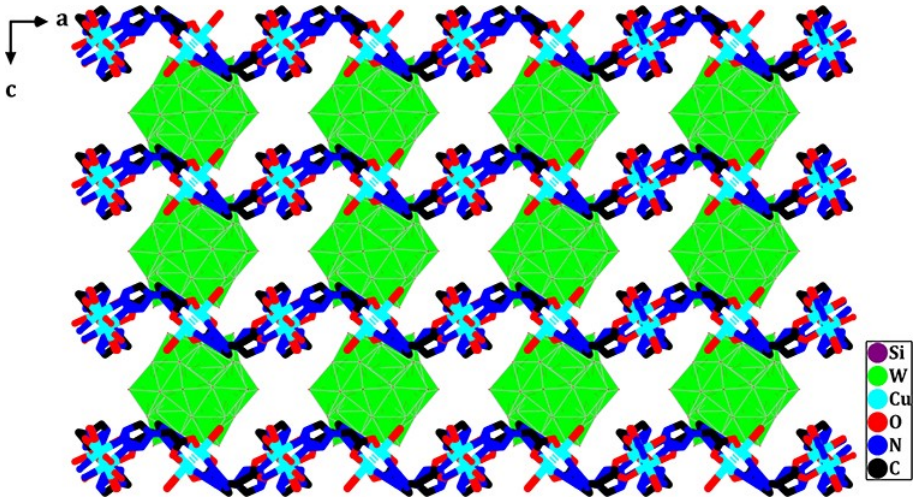

Fig. S11. The POM-based 3D supramolecular structure of **2** viewed from the *b* axis.

Section III. Supplementary Physical Characterizations

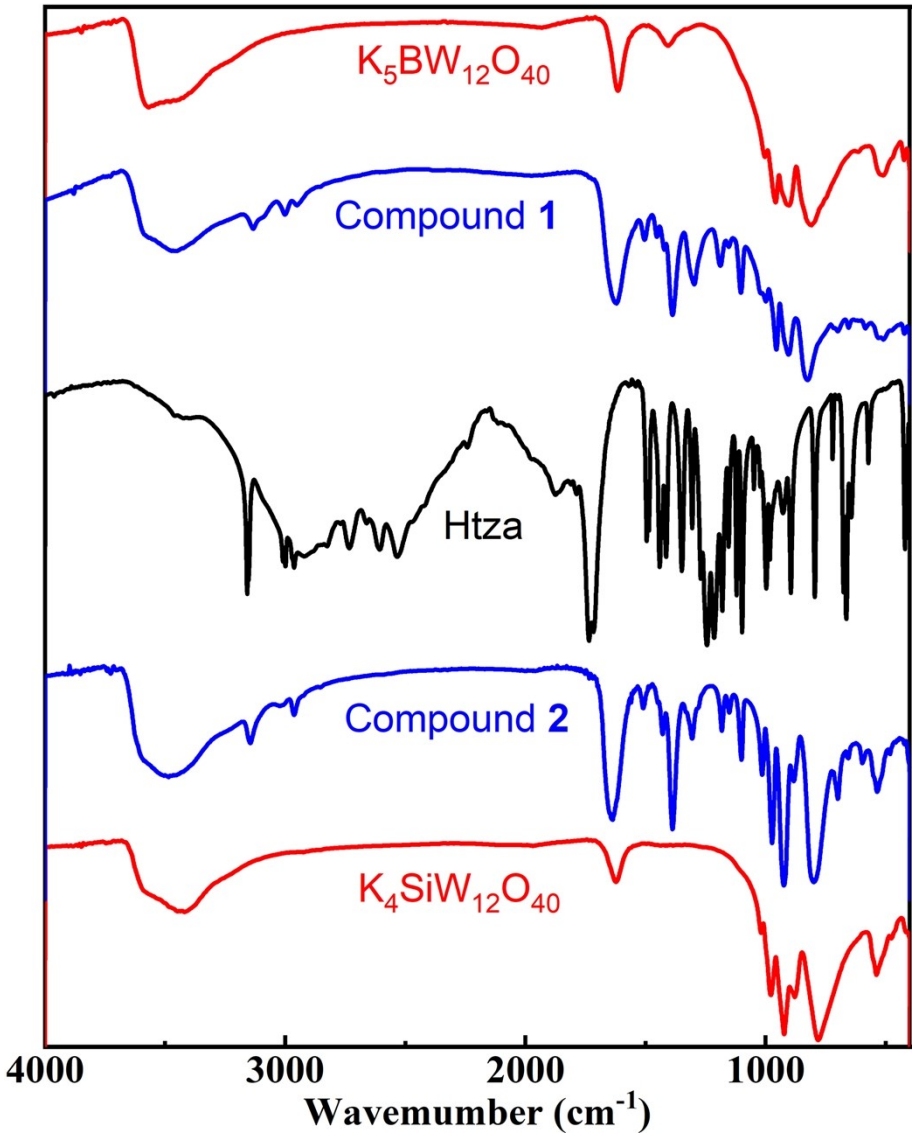

Fig. S12. IR spectra for **1, 2,** $K_5BW_{12}O_{40}$, $K_4SiW_{12}O_{40}$, and tetrazol-1-ylacetic acid.

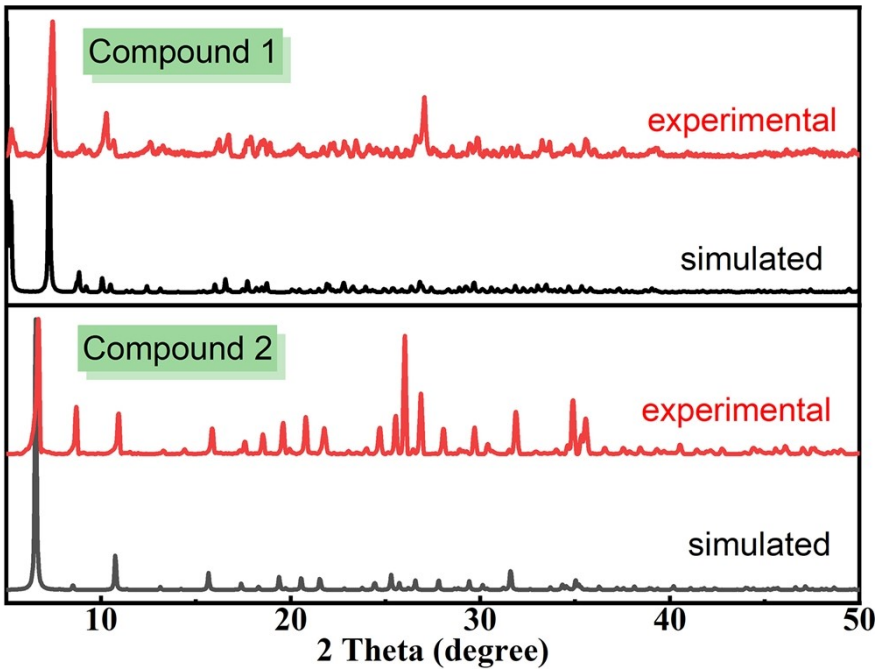

Fig. S13. The simulated and experimental PXRD patterns for **1** and **2.**

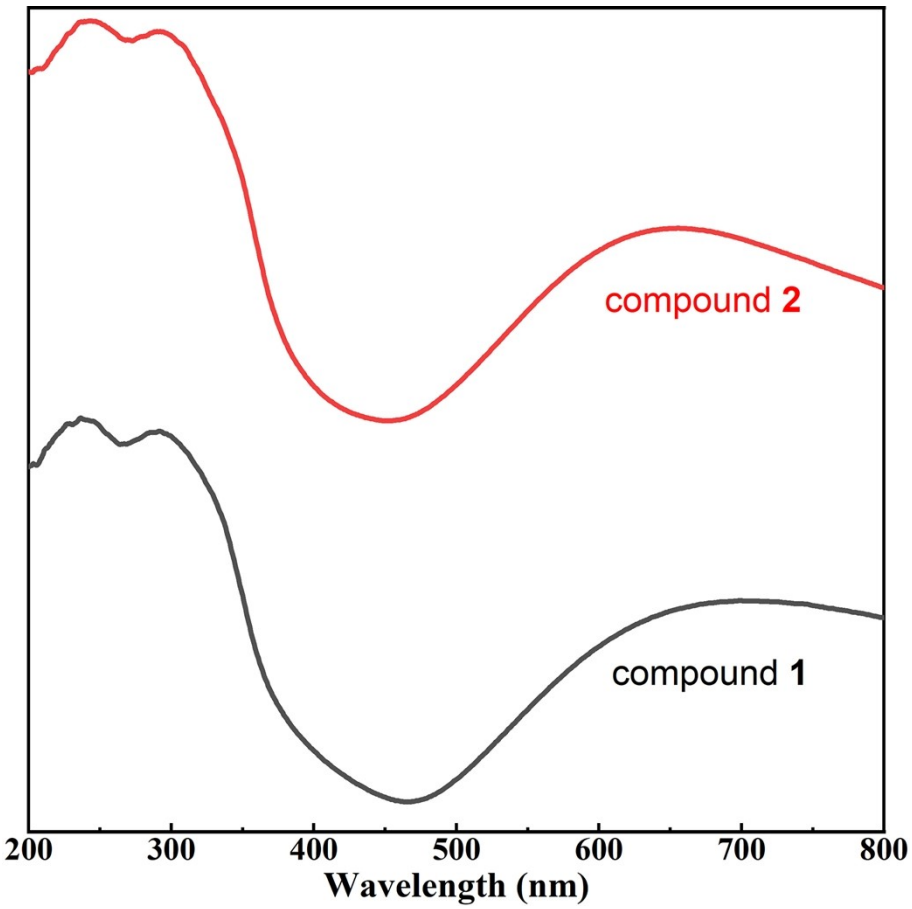

Fig. S14. UV−vis diffuse reflectance spectra of **1** and **2**.

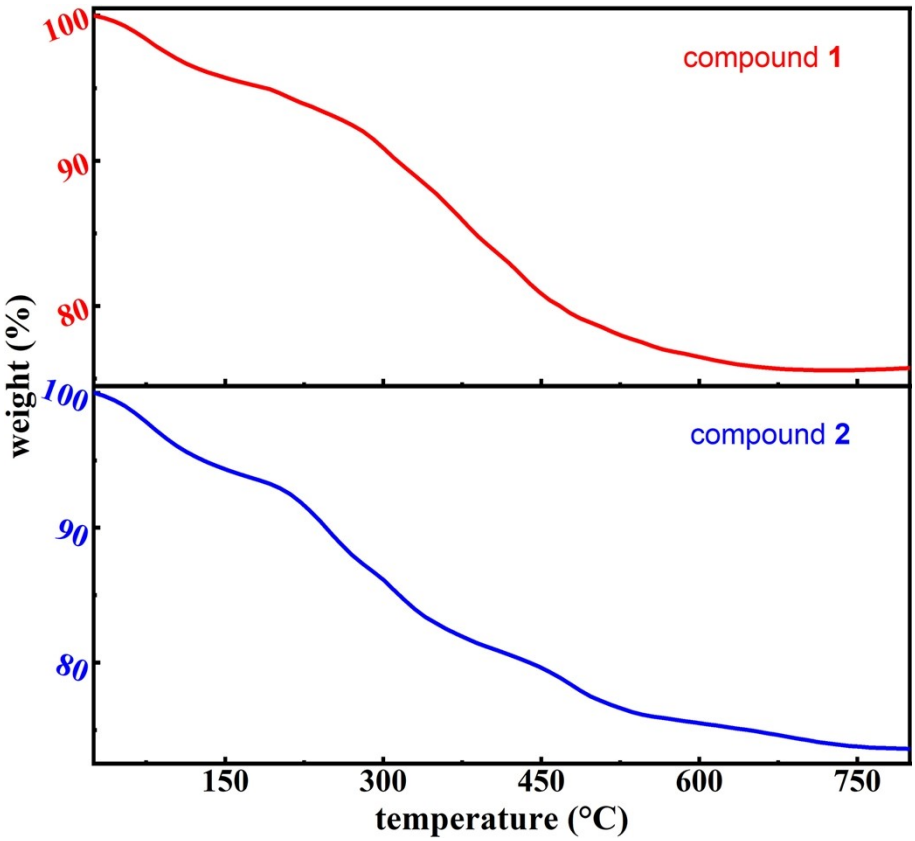

Fig. S15. The TGA curves of **1** and **2**.

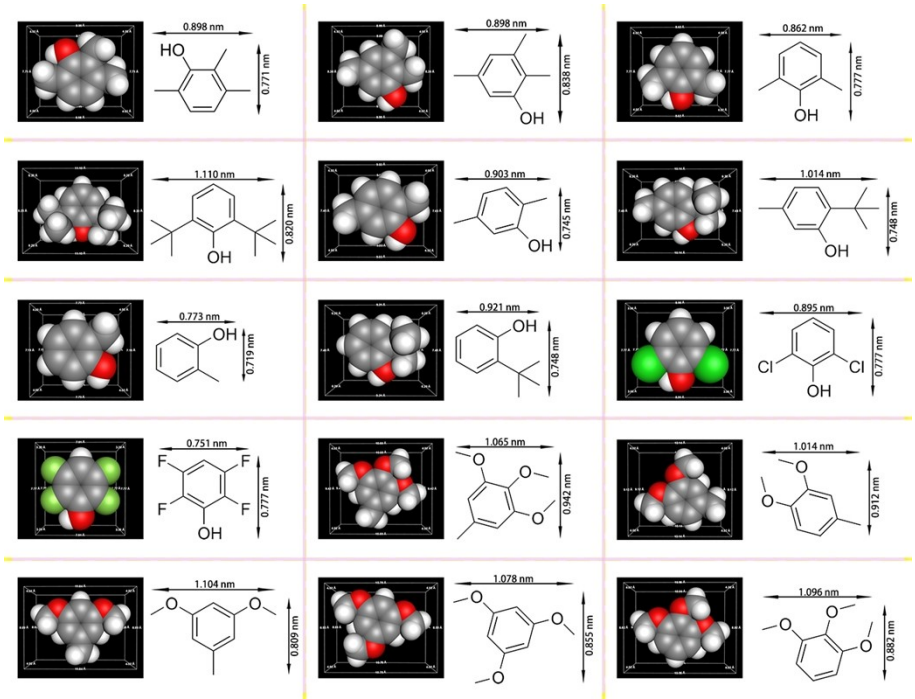

Fig. S16. The molecular sizes of different organic substrates. These molecular sizes are calculated based on the Corey-Pauling-Koltun（CPK) model.[S2]

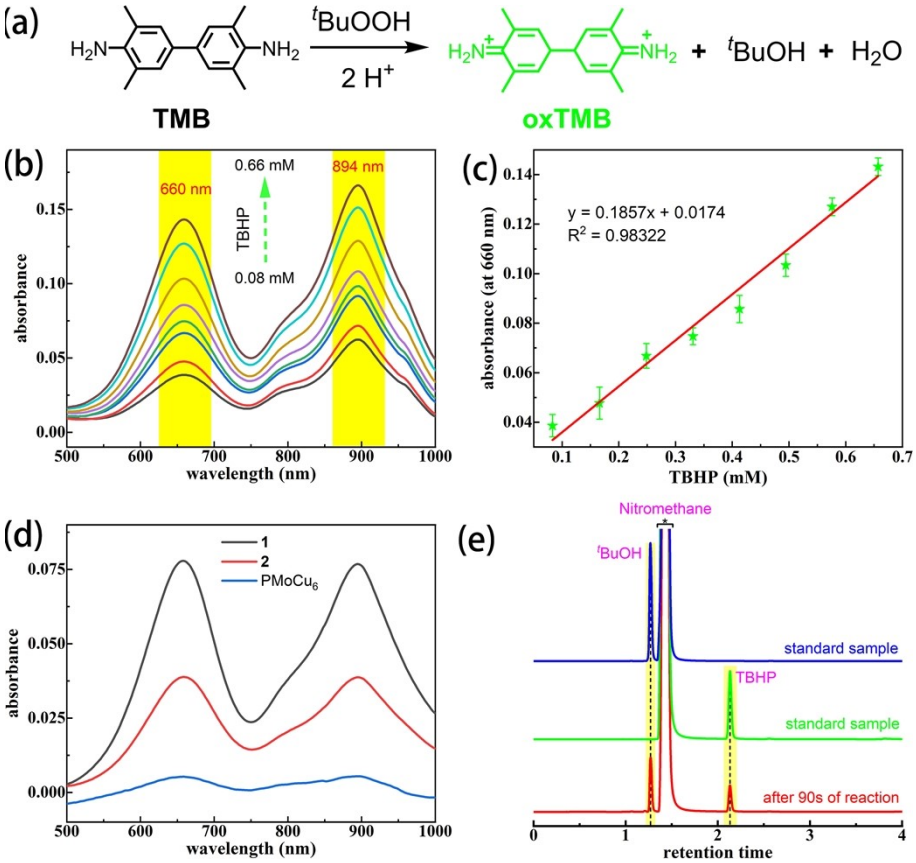

Fig. S17. The detection of oxidant. (a) The oxidation reaction of TMB in the presence of TBHP. (b) UV−vis spectra of TMB oxidation with various TBHP concentrations in buffer solution (pH~3.95). (c) The dose-response curve and the linear calibration plot for TBHP detection. (d) UV−vis spectra of TMB oxidation with the filtrate of TMP oxidation reaction catalyzed by compounds **1**-**2** and $PMoCu_6$ (the reaction conditions of TMP oxidation: 0.25 mmol of TMP, 0.15mol% of catalysts, 2.25 equivalent of TBHP, 0.5 mL MeCN at 60 ºC for 8 min for **1**, 10 min for **2**, and 30 min for $PMoCu_6$). (e) The GC-FID signals recording the TMB transformation process in the presence of TBHP (3.12 μmol of TMB, 2.03 μmol of TBHP, excessive 0.1M HCl, and 3 mL of nitromethane at 40 ºC for 2 min).

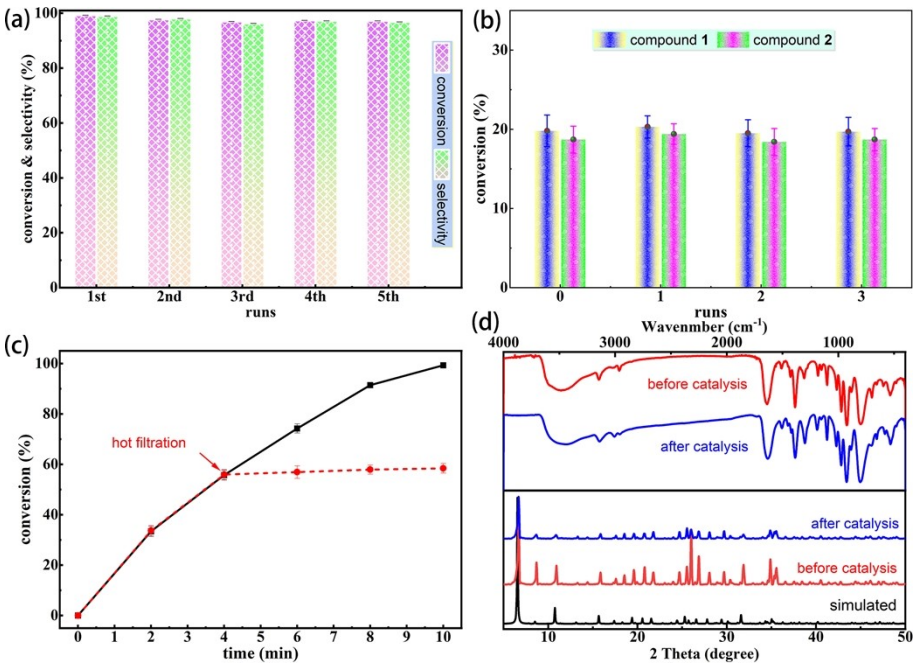

Fig. S18. The test of the heterogeneous nature and the stability of the catalyst **1** and **2**. (a) The recycle test for the oxidation of TMP to TMBQ using recovered **2**. (b) The recycle test of **1** and **2** in the kinetic regime (0.25 mmol of TMP, 0.15mol% of catalysts, 2.25 equivalent of TBHP, 0.5 mL MeCN at 60 ºC for 1 min). (c) Hot filtration test for TMP oxidation over **2** under optimal reaction conditions. (d) IR spectra and PXRD patterns for **2** before and after catalysis.

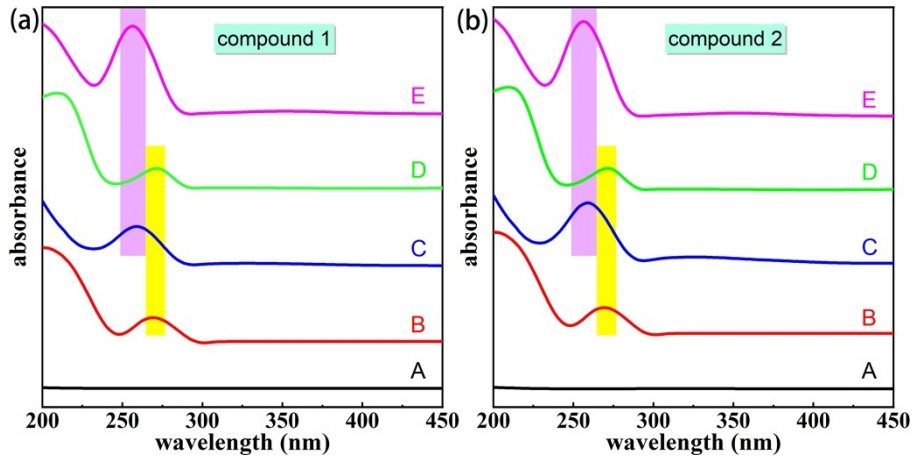

Fig. S19. The UV-vis spectra of TMP oxidation catalyzed by **1** and **2**: (A) the UV-vis spectra of filtrate after reaction for 8-10 min under the optimal conditions without substrate; (B) the UV-vis spectra of filtrate before reaction; (C) the UV-vis spectra of filtrate after reaction; (D) the UV-vis spectra of pure TMP; (E) the UV-vis spectra of pure TMBQ.

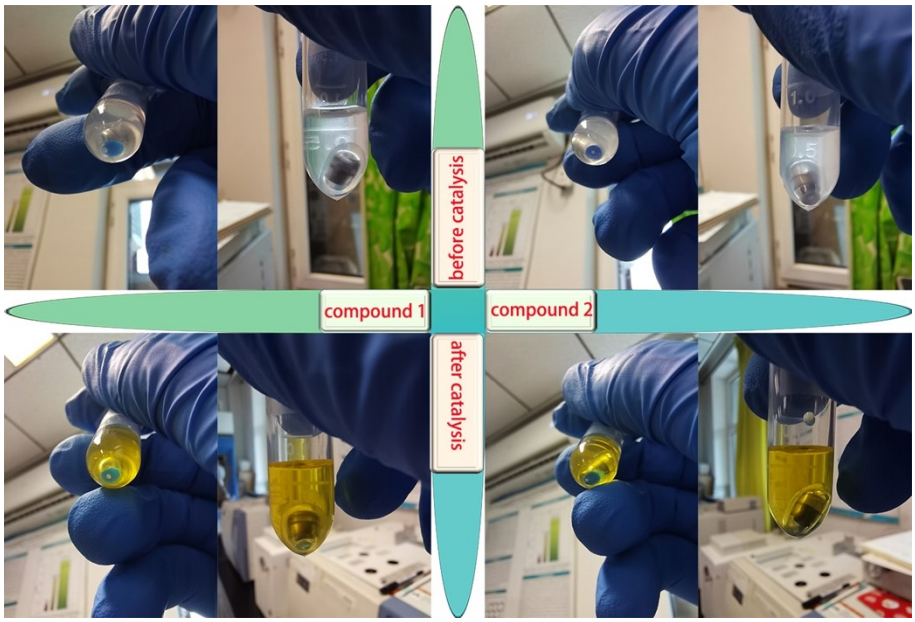

Fig. S20. The photographs of compound 1 and 2 before and after catalysis.

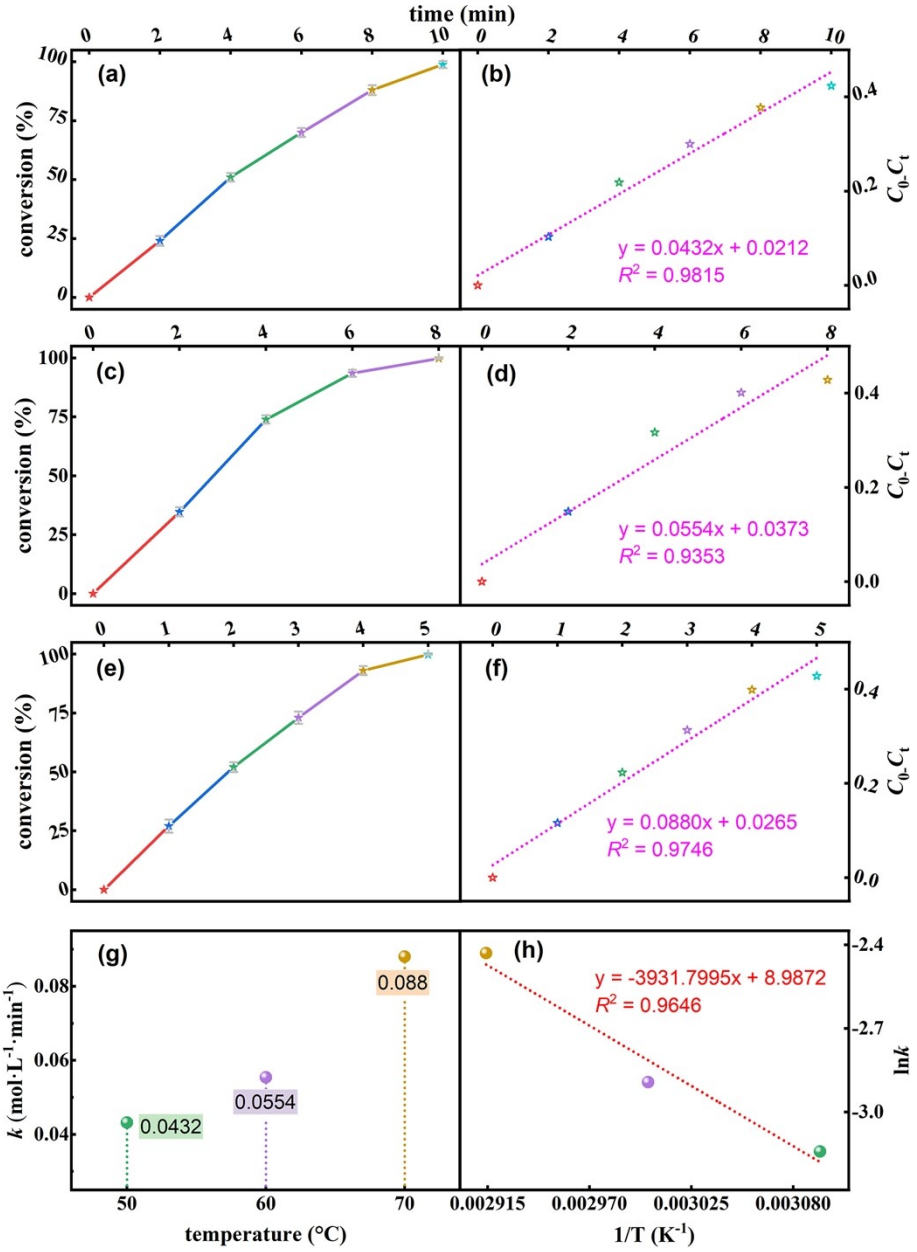

Fig. S21. Kinetic profiles of oxidation of TMP catalyzed by **1** with TBHP in CH_3CN. (a) Time profile curves and (b) first order kinetics fitting curves at 50 ℃. (c) Time profile curves and (d) first order kinetics fitting curves at 60 ℃. (e) Time profile curves and (f) first order kinetics fitting curves at 70 °C. (g) The corresponding *k* at different temperatures. (h) The Arrhenius−Eyring plot ($lnk = -(E_a/RT) + lnA$). C_0 and C_t represent the TMP concentration at the initial time and t min.

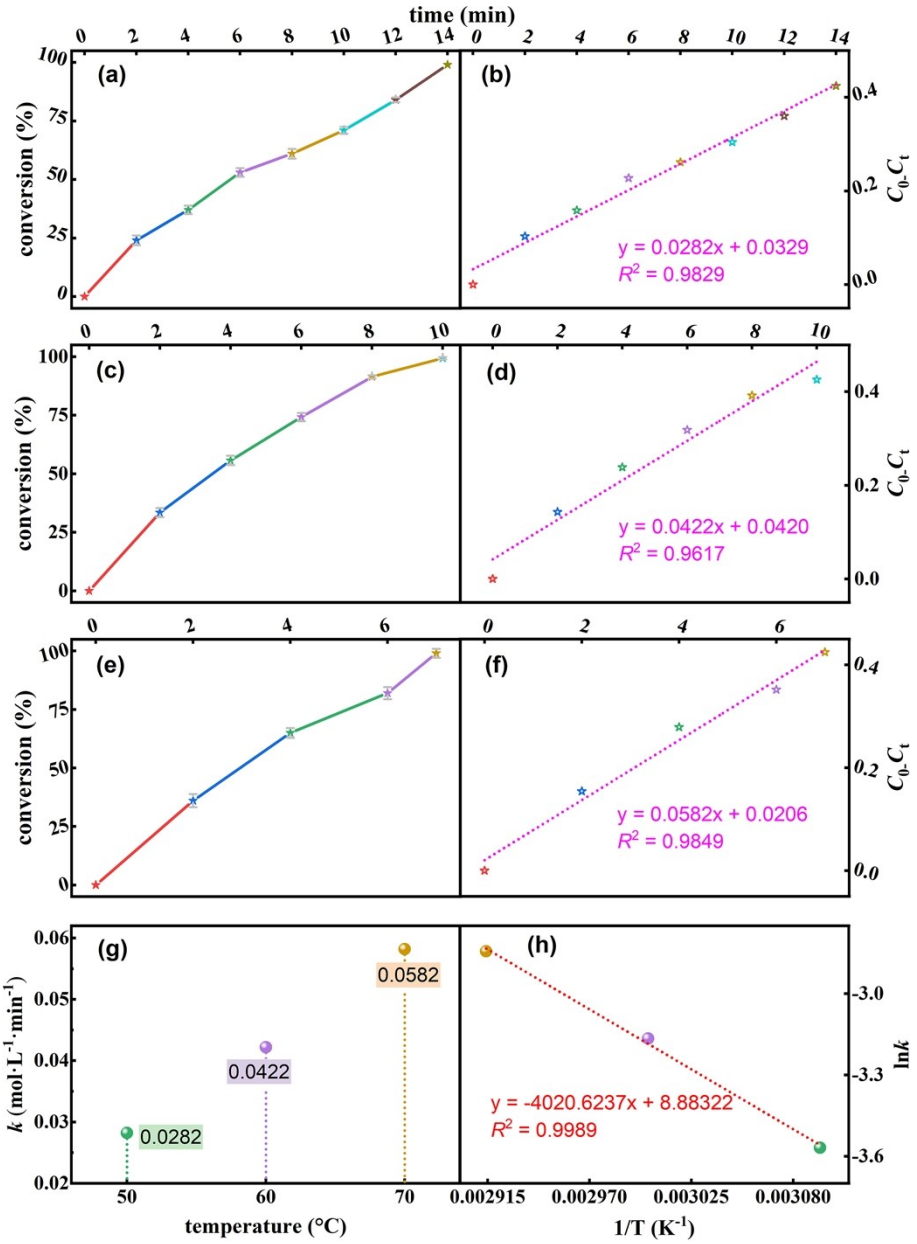

Fig. S22. Kinetic profiles of oxidation of TMP catalyzed by **2** with TBHP in CH_3CN. (a) Time profile curves and (b) first order kinetics fitting curves at 50 ℃. (c) Time profile curves and (d) first order kinetics fitting curves at 60 ℃. (e) Time profile curves and (f) first order kinetics fitting curves at 70 °C. (g) The corresponding k at different temperatures. (h) The Arrhenius−Eyring plot ($lnk = -(E_a/RT) + lnA$). C_0 and C_t represent the TMP concentration at the initial time and t min.

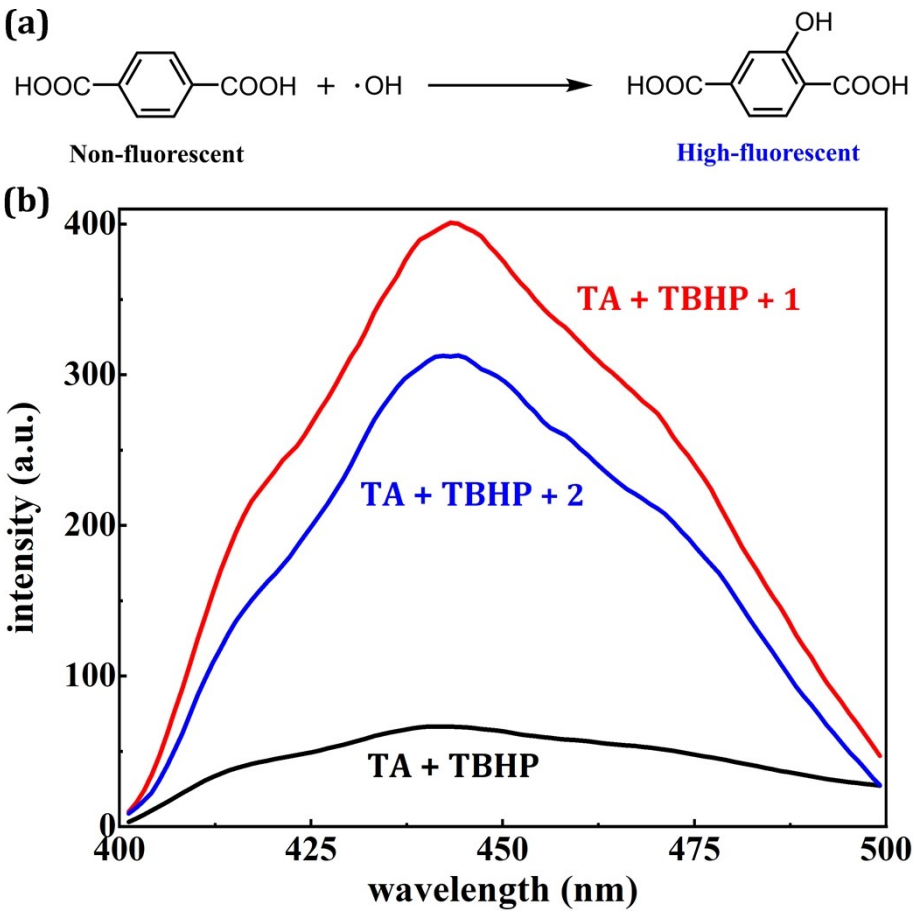

Fig. S23. The photoluminescence detection technology for probing hydroxyl radicals. (a) Hydroxyl radicals induced the conversion of non-fluorescent terephthalic acid (TA) to highly-fluorescent 2-hydroxyterephthalic acid. (b) Fluorescence spectra of TA solution (3×10^{-3} mol/L) in the absence and presence of catalysts with TBHP (300 mM). 0 mg catalyst, and 5 mg compounds 1-2 during photoluminescence probing, respectively.

Section IV. Supplementary Tables

Table S1. The oxidation of TMP to TMBQ catalyzed by **1**[a].

entry	catal. (μmol)	TBHP (mmol)	temp. (°C)	solvent (0.5 mL)	time (min)	con. (%)[b]	yield (%)[c]	TOF (h^{-1})[d]	TOF (h^{-1})[e]
1	0	0.55	60	MeCN	60	16.8	11.6	—	—
2	0.625	0	60	MeCN	60	trace	trace	—	—
3	0	0	60	MeCN	60	trace	trace	—	—
4	0.625	0.625	r.t.	MeCN	100	>99	86.7	240	208
5	0.625	0.625	40	MeCN	60	>99	91.9	400	368
6	0.625	0.625	50	MeCN	10	>99	96.0	2400	2304
7	0.625	0.625	60	MeCN	8	>99	98.6	3000	2958
8	0.625	0.625	70	MeCN	5	>99	97.9	4800	4699
9	0.625	0.625	80	MeCN	4	>99	97.1	6000	5826
10	0.5	0.625	60	MeCN	8	>99	98.9	3750	3709
11	0.375	0.625	60	MeCN	8	>99	>99	5000	5000
12	0.25	0.625	60	MeCN	10	>99	94	6000	5640
13	0.375	0.50	60	MeCN	8	97.9	94.8	4895	4740
14	0.375	0.55	60	MeCN	8	>99	>99	5000	5000
15	0.375	0.70	60	MeCN	7	>99	>99	5714	5714
16[f]	0.375	0.55	60	MeCN	6	89.4	84.1	4470	4205
17[g]	0.375	1 atm	60	MeCN	180	trace	trace	—	—
18[h]	18.75	27.5	60	MeCN	12	>99	94.5	3333	3150

[a]Reaction conditions: 0.25 mmol of TMP. [b]Results determined by GC using naphthalene as internal standard. [c]Yield to TMBQ. [d]Turnover frequency (TOF) = (mol of TMP consumed)/(mol of the catalyst used × reaction time). [e]TOF = (mol of TMBQ yielded)/(mol of the catalyst used × reaction time). [f]30% H_2O_2 as oxidant. [g]O_2 as oxidant. [h]enlarged-scale test: 12.5 mmol of TMP, 20 mL of solvent.

Table S2. The oxidation of TMP to TMBQ catalyzed by **1** under different solvent[a].

entry	solvent (0.5 mL)	con. (%)[b]	yield (%)[c]	TOF (h^{-1})[d]	TOF (h^{-1})[e]
1	MeOH	58.9	57.1	2945	4315
2	EtOH	57.0	48.5	2850	4250
3	i-PrOH	54.8	53.8	2740	4655
4	*n*-BuOH	57.6	56.7	2880	4665
5	Acetone	96.0	92.0	4800	4600
6[f]	DMF	97.9	73.8	4895	3690
7[f]	DMSO	97.9	83.6	4895	4180
8	THF	75.1	75.1	3755	3755
9	Pyridine	98.8	96.8	4940	4840
10	DCM	54.7	44.8	2735	2240
11	Chloroform	6.17	4.07	308.5	203.5
12	Nitromethane	95.7	95.7	4785	4785
13	n-Hexane	26.5	19.1	1325	955
14	Cyclohexane	12.2	10.5	610	525
15	n-Octane	13.7	11.8	685	590
16	Benzene	12.5	10.1	625	505
17	Toluene	3.26	trace	163	—
18	Ethylbenzene	10.5	6.42	525	321
19	Mesitylene	5.84	trace	292	—
20	TFT	2.50	trace	125	—

[a]Reaction conditions: 0.25 mmol of TMP, 0.15mol% of catalysts, 2.2 equivalents of TBHP, 60 °C and reaction time: 8 min. [b]Results determined by GC using naphthalene as internal standard. [c]Yield to TMBQ. [d]TOF = (mol of TMP consumed)/(mol of the catalyst used × reaction time). [e]TOF = (mol of TMBQ yielded)/(mol of the catalyst used × reaction time). [f]Homogeneous system.

Table S3. Comparison of representative systems for TMP oxidation.

entry	catal.	oxidant	temp. (°C)	time (min)	con. (%)	sel. (%)	TOF (h^{-1})	reaction system	ref.
1	**1**	TBHP	60	8	>99	>99	5000	heterogeneous	this work
2	**2**	TBHP	60	10	>99	98.7	4000	heterogeneous	
3	**$PMoCu_6$**	H_2O_2	80	5	>99	>99	2400	heterogeneous	S3
4	**$PWCu_6$**	H_2O_2	80	6	>99	>99	2000	heterogeneous	S3
5	**$PMoCu_3$**	H_2O_2	80	8	>99	>99	1500	heterogeneous	S3
6	**$PWCu_3$**	H_2O_2	80	15	>99	>99	800	heterogeneous	S3
7	**$PWCu_4$**	H_2O_2	60	20	>99	>99	300	heterogeneous	S4
8	**$PWCu_4$**	H_2O_2	80	15	>99	>99	396	heterogeneous	S4
9	**$PWCu_{17}$**	H_2O_2	60	10	>99	96	576	heterogeneous	S4
10	**$PWCu_{17}$**	H_2O_2	80	8	>99	95	742	heterogeneous	S4
11	**γ-$PW_{10}V_2$**	H_2O_2	80	4	>99	>99	500	homogeneous	S5
12	**γ-$PW_{10}V_2$**	H_2O_2	80	2	>99	78	1000	homogeneous	S5
13	**$PW_{11}Ti$**	H_2O_2	80	30	90	45	60	homogeneous	S6
14	**$PW_{11}Zr$**	H_2O_2	80	60	90	30	18	homogeneous	S7
15	**γ-$PW_{10}V_2$/CNTs**	H_2O_2	60	15	>99	>99	500	heterogeneous	S8
16	**FePcS/MIL-101**	TBHP	30	15	95	57	380	heterogeneous	S9
17	**Ti/MIL-125**	H_2O_2	80	15	70	100	90	heterogeneous	S10
18	**Ti/SiO_2**	H_2O_2	80	30	100	98	126	heterogeneous	S11
19	**Ti_2/SiO_2**	H_2O_2	80	30	99	96	114	heterogeneous	S12
20	**Ti_4/SiO_2**	H_2O_2	80	30	100	97	120	heterogeneous	S12
21	**Ti/Si-EISA**	H_2O_2	80	40	100	100	138	heterogeneous	S13
22	**Ti/SBA-15**	H_2O_2	80	60	100	100	204	heterogeneous	S14
23	**TS-1**	H_2O_2	80	180	>99	96	10	heterogeneous	S15
24	**Cu/SBA-15**	H_2O_2	80	40	100	98	9660	heterogeneous	S16
25	**NBND**	H_2O_2	60	360	>99	97	—	heterogeneous	S17
26	**OLC-1**	TBHP	80	720	>99	82.5	—	heterogeneous	S18
27	**$CuCl_2$**	H_2O_2	60	8	>99	90	250	homogeneous	S4

Table S4. Comparison of TMP oxidation catalyzed by compounds **1**-**2** and $PMoCu_6$ with TBHP as oxidant[a].

catal	time (min)	con. (%)[b]	sel. (%)	TOF (h^{-1})[c]	oxidant efficiency (%)[d]
1	8	>99	>99	5000	94.25
2	10	>99	98.7	4000	90.87
$PMoCu_6$[e]	30	98.4	97.4	1312	87.35
1[f]	5	94.4	92.8	2266	76.45
2[f]	5	94.5	91.5	2268	73.87
$PMoCu_6$[f]	5	>99	99	2400	82.77

[a]Reaction conditions: 0.25 mmol of TMP, 0.15mol% of catalysts, 2.2 equivalents of TBHP, 0.5 mL MeCN, and 60 ºC. [b]Results determined by GC using naphthalene as internal standard. [c]Turnover frequency (TOF) = (mol of TMP consumed)/(mol of the catalyst used × reaction time). [d]TBHP efficiency (%) = 100 × (mol of TBHP consumed in the formation of TMBQ/mol of TBHP converted). The calculation results are as follows. [e]The catalyst used is from reference S3, but the reaction conditions are the same as **1** and **2**. [f]Reaction conditions (0.25 mmol of TMP, 0.50mol% of catalysts, 4.0 equivalents of H_2O_2, 0.5 mL MeCN, and 80 ºC.) or results are quoted from reference S3.

*Calculation of the efficiency of the oxidant for **1**:*

- The mol of TBHP consumed in the formation of TMBQ (yield: >99 %) from 0.25 mmol TMP = 0.5 mmol
- Total mol of TBHP has been originally used for the reaction = 0.55 mmol;
- The remaining mol of TBHP in the system after the reaction = 0.0195 mmol
- TBHP efficiency (%) = 100 × [0.5/(0.55-0.0195)] = 94.25%

*Calculation of the efficiency of the oxidant for **2**:*

- The mol of TBHP consumed in the formation of TMBQ (yield: 98.7 %) from 0.25 mmol TMP = 0.4935 mmol
- Total mol of TBHP has been originally used for the reaction = 0.55 mmol;
- The remaining mol of TBHP in the system after the reaction = 0.0069 mmol
- TBHP efficiency (%) = 100 × [0.4935/(0.55-0.0069)] = 90.87%

Calculation of the efficiency of the oxidant for $PMoCu_6$:

- The mol of TBHP consumed in the formation of TMBQ (yield: 95.84 %) from 0.25 mmol TMP = 0.4792 mmol

- Total mol of TBHP has been originally used for the reaction = 0.55 mmol;
- The remaining mol of TBHP in the system after the reaction = 0.0014 mmol
- TBHP efficiency (%) = 100 × [0.4792/(0.55-0.0014)] = 87.35%

Table S5. Investigated the change of the content of W atom and Cu atom in the catalyst system after the oxidation reaction of TMP with ICP-AES.

The change of catalyst quality before and after reaction[a]				
	before		after	
	1	**2**	**1**	**2**
total mass/mg	1.6	1.7	1.5	1.5
The metal content in filtrate after reaction[b]				
	W		Cu	
	1	**2**	**1**	**2**
c/mg·mL^{-1}	4.04×10^{-4}	6.11×10^{-4}	1.01×10^{-4}	2.53×10^{-4}

[a]Reaction conditions: 0.25 mmol of TMP, 0.15mol% of catalysts, 2.2 equivalents of TBHP, 0.5 mL MeCN, 60 ºC and reaction time: 8 min for **1** and 10 min for **2**. The loss of total mass before and after catalysis may be caused by some inevitable physical factors in the recovery process. [b]After the reaction filtrate was rotary evaporated, 3 mL of ultrapure water was added and stirred at 60 ºC for 10 minutes, and then filtered with a syringe filter to obtain the filtrate.

Table S6. Crystal data and structure refinement for **1** and **2**.

Compound	**1**	**2**
CCDC number	2052783	2069056
Formula	$C_{18}H_{48}N_{24}K_3Cu_3BW_{12}O_{66}$	$C_{18}H_{67}N_{24}K_3Cu_3SiW_{12}O_{76}$
Formula weight	4181.73	4378.16
T (K)	190(2)	296(2)
Crystal system	Trigonal	Trigonal
Space group	*R-3*	*P-3*
a (Å)	35.1668(9)	15.570(3)
b (Å)	35.1668(9)	15.570(3)
c (Å)	20.2270(6)	10.337(3)
α (˚)	90	90
β (˚)	90	90
γ (˚)	120	120
V (Å^3)	21663.5(12)	2170.3(11)
Z	9	1
μ (mm^{-1})	15.153	16.836
Index ranges	$-41 \le h \le 36$ $-41 \le k \le 41$ $-24 \le l \le 23$	$-15 \le h \le 18$ $-18 \le k \le 18$ $-12 \le l \le 12$
Reflections collected	39054	11390
Independent reflections	8468	2548
R_{int}	0.0503	0.0457
Data/restraints/parameters	8468/111/646	2554/36/233
GOF on F^2	1.350	1.075
R_1, wR_2 [$I > 2\sigma(I)$]	0.0775, 0.1653	0.0445, 0.1258
R_1, wR_2 (all data)	0.0808, 0.1667	0.0475, 0.1284

$R_1 = \Sigma||F_o| - |F_c||/\Sigma|F_o|$. $wR_2 = \Sigma[w(F_o^2 - F_c2)^2]/\Sigma[w(F_o^2)^2]^{1/2}$

Section V. References

S1. C. Rocchiccioli-Deltcheff, M. Fournier, R. Franck and R. Thouvenot, *Inorg. Chem.*, 1983, **22**, 207−216.

S2. Z. Zhang, Y. W. Liu, H. R. Tian, X. H. Li, S. M. Liu, Y. Lu, Z. X. Sun, T. Liu and S. X. Liu, *Matter*, 2020, **2**, 250-260.

S3. S. Z. Chang, Y. H. Chen, H. Y. An, Q. S. Zhu, H. Y. Luo and T. Q. Xu, *ACS Appl. Mater. Interfaces*, 2021, **13**, 21261−21271.

S4. S. Z. Chang, H. Y. An, Y. H. Chen, Y. J. Hou, J. Zhang and Q. S. Zhu, *ACS Appl. Mater. Interfaces*, 2019, **11**, 37908−37919.

S5. I. D. Ivanchikova, N. V. Maksimchuk, R. I. Maksimovskaya, G. M. Maksimov and O. A. Kholdeeva, *ACS Catal.*, 2014, **4**, 2706−2713.

S6. O. A. Kholdeeva, T. A. Trubitsina, G. M. Maksimov, A. V. Golovin and R. I. Maksimovskaya, *Inorg. Chem.*, 2005, **44**, 1635−1642.

S7. O. A. Kholdeeva, G. M. Maksimov, R. I. Maksimovskaya, M. P. Vanina, T. A. Trubitsina, D. Y. Naumov, B. A. Kolesov, N. S. Antonova, J. J. Carbo and J. M. Poblet, *Inorg. Chem.*, 2006, **45**, 7224−7234.

S8. V. Y. Evtushok, A. Suboch, O. Y. Podyacheva, O. A. Stonkus, V. I. Zaikovskii, Y. A. Chesalov, L. S. Kibis and O. A. Kholdeeva, *ACS Catal.*, 2018, **8**, 1297−1307.

S9. O. V. Zalomaeva, K. A. Kovalenko, Y. A. Chesalov, M. S. Mel'gunov, V. I. Zaikovskii, V. V. Kaichev, A. B. Sorokin, O. A. Kholdeeva and V. P. Fedin, *Dalton Trans.*, 2011, **40**, 1441−1444.

S10. I. D. Ivanchikova, J. S. Lee, N. V. Maksimchuk, A. N. Shmakov, Y. A. Chesalov, A. B. Ayupov, Y. K. Hwang, C. H. Jun, J. S. Chang and O. A. Kholdeeva, *Eur. J. Inorg. Chem.*, 2014, **2014**, 132−139.

S11. O. A. Kholdeeva, I. D. Ivanchikova, M. Guidotti and N. Ravasio, *Green Chem.*, 2007, **9**, 731−733.

S12. O. A. Kholdeeva, I. D. Ivanchikova, M. Guidotti, C. Pirovano, N. Ravasio, M. V. Barmatova and Y. A. Chesalov, *Adv. Synth. Catal.*, 2009, **351**, 1877−1889.

S13. I. D. Ivanchikova, M. K. Kovalev, M. S. Mel'gunov, A. N. Shmakov and O. A. Kholdeeva, *Catal. Sci. Technol.*, 2014, **4**, 200−207.

S14. M. Selvaraj, *Catal. Sci. Technol.*, 2014, **4**, 2674−2684.

S15. J. Zhou, Z. L. Hua, X. Z. Cui, Z. Q. Ye, F. M. Cui and J. L. Shi, *Chem. Commun.*, 2010, **46**, 4994−4996.

S16. M. Selvaraj and M. A. Assiri, *Dalton Trans.*, 2019, **48**, 3291−3299.

S17. Y. M. Lin, Z. G. Liu, Y. M. Niu, B. S. Zhang, Q. Lu, S. H. Wu, G. Centi, S. Perathoner, S. Heumann, L. H. Yu and D. S. Su, *ACS Nano*, 2019, **13**, 13995−14004.

S18. Y. M. Lin, B. Li, Z. B. Feng, Y. A. Kim, M. Endo and D. S. Su, *ACS Catal.*, 2015, **5**, 5921−5926.